Wind design spectra for generalisation

Martinez-Vazquez, Pedro

Document Version
Peer reviewed version

Wind Design Spectra for Generalisation

P Martinez-Vazquez[1]

School of Engineering, University of Birmingham, B15 2TT, United Kingdom

Abstract. Previous research has shown that wind acceleration components produce a signal that can vibrate single-degree of-freedom oscillators, whose dynamic responses enable to configure design spectra for structures subject to wind. These wind design spectra present an alternative method for evaluating the dynamic response of structures to wind and are a suitable tool for running modal analyses. Here, a generalised method for producing wind design spectra is proposed. The method consists of scaling existing spectra to adjust to a wider range of building properties and terrain conditions. The modelling technique is tested on a benchmark building to prove that its results are consistent with experimental evidence reported in the past.

Key words: wind design spectra; wind loading; wind aerodynamics; performance-based design

1. Introduction

Wind design spectra developed as an alternative method for determining the dynamic response of structures subject to wind. Martinez-Vazquez (2016) proposed a series of equations to determine the dynamic response of single-degree-of-freedom (SDOF) systems subject to wind-induced accelerations. Wind design spectra are graphic representations of the systems' response acceleration versus their fundamental vibrational period. The method is analogous to the spectral methods proposed by Esteva and Rosenblueth (1964), Newmark and Hall (1982), Chopra (1995), and Priestley (2000), and others, which over time contributed to shaping the performance-based design philosophy that earthquake-resistant design codes across the globe now embrace. An equivalent design philosophy is now starting to develop in wind engineering, as shown in Petrini and Ciampoli (2012) and Huang et al. (2015). These build on previous efforts to develop spectral techniques that consider wind loading. Solary (1988, 1989) recognised that such techniques require suitable aerodynamic admittance and cross-correlation functions to characterise wind-structure interactions. Although the Equivalent Wind Spectral Technique proposed by Solary (1988, 1989) identified generalised wind loading scenarios that facilitate the accurate estimation of peak structural responses, it did not chart pseudo-spectral accelerations against natural periods or frequencies of vibration of single oscillators, as required to run modal analyses. Martinez-Vazquez (2016) provided such a tool, alongside evidence of how the spectral approximation, once applied to multiple-degree-of-freedom systems, produces results that are compatible with numerical and experimental evidence.

Other approaches to estimate the dynamic response of structures subject to wind have focused on the Gust Load Factor proposed by Davenport (1967). Those include, but are not restricted to, the Load Response Correlation (Kapersky, 1992), Generalised Gust Factor (Piccardo and Solari 2000), Gust Response Factor (Zhou and Kareem 2001), Effective Static Load Distribution (Holmes 2002), Equivalent Static Wind Load (Chen and Kareem 2004; Chen and Zhou 2007, Gong and Chen, 2015, Patruno et al. 2017), and the Universal Equivalent Static Load (Tamura and Katsumura 2012, Sun et al. 2016). These simulate the mean and background dynamic response components by means of superimposed static load configurations weighted by peak factors. The relatively new wind spectral approach to wind analysis is not unrelated to those techniques, as it can also disassemble into background and resonant components

---

[1] Corresponding author, Ph.D., E-mail: p.vazquez@bham.ac.uk

that reflect the cross-correlation properties of wind gusts, such as those proposed in Vickery (1970) and Tanaka and Lawen (1986). The classical and spectral techniques diverge in that the former produces quasi-static force fields that act directly on structures, whereas the latter yields generalised forces that are used to vibrate SDOF systems whose dynamic responses conform design spectra.

The present paper scrutinises the multi-factorial nature of wind-structure interactions in light of the spectral approach. It shows that most of the controlling parameters that define wind loading exhibit nonlinear relationships with buildings' dynamic response, while a few other factors can escalate design spectra more directly. The study includes the development of a regression model to reproduce the otherwise on-a-single-case-basis estimated wind design spectra, as a first step towards their generalisation.

The paper is organised as follows: Section 2 gives an overview of the spectral method; Section 3 identifies the parameters that determine wind-structure interactions; Section 4 discusses the regression model; Section 5 applies real and simulated design spectra to a case study; and Section 6 consists of some final conclusions.

2. Wind design spectra formulation

Stage 1: Spectrum of Acceleration

In this Stage, we reflect on the physical relationship between force and acceleration, as per Newton's Second Law, to progressing force into its equivalent spectrum of acceleration. This establishes the basic framework on which wind design spectra develop.

Eq. (1) translates dynamic wind velocity components into a force acting on point-like structures. It uses the wind power spectrum, $S_u(n)$ affected with the quantity q^2, as discussed in Dyrbye and Hansen (1997). Since $F = \frac{1}{2}\rho C_D A U_T^2$ while $U_T^2 = (U + u)^2 = U^2 + 2Uu + u^2$, where U_T is the total wind velocity, A is the area exposed, U is the mean value, u is the turbulent velocity components, and F is the force exerted on bluff bodies, it follows that $2Uu + u^2 \cong u(2U + \sigma_u)$, where σ_u is the *rms* of wind speed, hence $q = \frac{1}{2}\rho C_D A(2U + \sigma_u)$. On that basis, the spectrum of wind acceleration takes the form given in Eq. (2), where m represents the mass of the discrete system. In this context, $S_A(n)$ provides input acceleration, the same way that $S_F(n)$ would provide input force generated by wind.

$$S_F(n) = q^2 S_u(n) \tag{1}$$

$$S_A(n) = \left(\frac{q}{m}\right)^2 S_u(n) \tag{2}$$

$$H(n) = \frac{1}{K\sqrt{(1-r^2)^2 + 4\xi^2 r^2}} \tag{3}$$

$$J(n) = \frac{1}{\sqrt{(1-r^2)^2 + 4\xi^2 r^2}} \tag{4}$$

Stage 2: Mechanical Admittance

Shifting from input to output (structural) acceleration requires a suitable transfer function. We thus depart from the classical force-displacement relationship to identify by analogy the function that converts input to output acceleration.

Let us consider the force-displacement relationship $|H(n)|^2 = S_d(n) / S_F(n)$, where $|H(n)|^2$ transfers the force spectrum $S_F(n)$ generated by the wind gust of frequency n, into spectral

displacement $S_d(n)$ (see Gould and Abu-Sitta, 1980). The square root of the area defined by $S_d(n)$ provides the *rms* of dynamic displacement. Note that Eq. (3) defines $H(n)$ in terms of stiffness (K), fraction of critical damping (ξ), and $r = {}^n/_{n_0}$ where n_0 symbolises the fundamental frequency of the system. In calculating $\frac{S_F(n)}{m^2}|J(n)|^2 = 16\pi^4 n^4 S_d(n)$ and re-arranging, one obtains $\frac{S_F(n)}{S_d(n)}|J(n)|^2 = 16\pi^4 n^4 m^2 = \frac{|J(n)|^2}{|H(n)|^2}$, which reveals $J(n) = KH(n)$ as the sought acceleration transfer function. This function is given in Eq. (4) and illustrated in Fig. 1 for various damping levels.
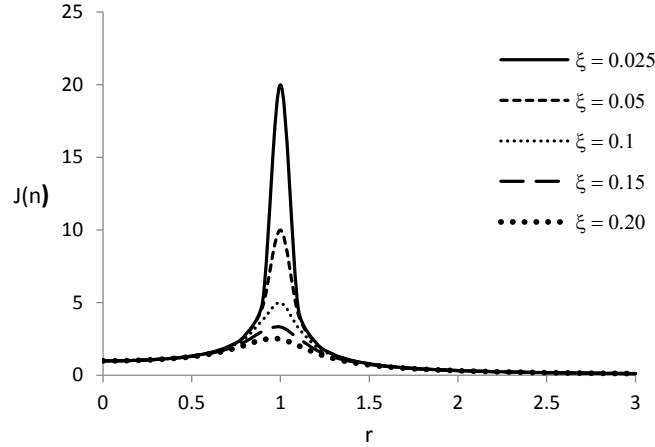

Fig. 1 Transfer function $J(n)$ for different damping levels.

Eqs. (2) and (4) are thus analogous to Eqs. (1) and (3). Either pair represent inputs to the dynamical system and related mechanical admittance, in terms of acceleration and force, respectively. These are valid for point-like structures.

Stage 3: Cross Spectrum of Acceleration and its Generalisation

In dealing with two-dimensional structures, one has to consider the spatial nature of wind gusts. That property is reflected in the real part of the cross-spectrum of two longitudinal turbulence components, which expressed as in Dyrbye and Hansen (1997) - after Davenport (1977), gives Eq. (5) below,

$$\chi(z,n) = e^{-\frac{n}{1/2[U(z_i)+U(z_j)]}\sqrt{(C_y \Delta_y)^2 + (C_z \Delta_z)^2}} \tag{5}$$

In these equation, the horizontal and vertical distances between two points i, j located at coordinates $\{y_i, z_i\}$ and $\{y_j, z_j\}$ are denoted by Δ_y and Δ_z, respectively; $\phi(z)$ is the modal amplitude at height z, and C_k is a decay constant along direction k. Typical values of C_k fall within the range 1–10, while $U(z)$ can be approximated with $U(z) = U({}^z/_{z_r})^\alpha$, where z_r is the reference height and α can take values of 0.12, 0.16, 0.22 and 0.3 for Terrain Types I, II, III and IV, respectively.

It follows that, by combining the spectrum of acceleration given in Eq. (2) and the cross-spectrum of longitudinal turbulence components, as expressed in Eq. (5), one defines the cross power spectrum of acceleration $S_{A_{ij}}(z,n)$ quoted in Eq. (6). Noting that this spectrum incorporates the function $\psi(z)$ to account for the variation of turbulence with height.

3

$$S_{A_{ij}}(z,n) = \frac{S_A(n)}{A^2} \psi(z) e^{-\frac{n}{1/2[U(z_i)+U(z_j)]}\sqrt{(C_y\Delta_y)^2+(C_z\Delta_z)^2}} \tag{6}$$

$$S_{cu}(n) = \iint_A \phi(z_i)\phi(z_j)S_{A_{ij}}(z,n)dy_i dy_j dz_i dz_j \tag{7}$$

The integration of Eq. (6) across the area exposed to wind flow, leads to the power spectral density of the generalised input acceleration $S_{cu}(n)$ given in Eq. (7) -. where the fundamental modal shape can take the form $\phi(z) = \left(z/H\right)^\beta$ with H representing the vertical dimension of A, and β taking a value within the range 1–1.5.

Stage 4: Wind Design Spectrum
Finally, once Eq. (7) provides the acceleration inputted to a system in a generalised form, we proceed to integrate it in two parts, one to determine the background response acceleration and the other to find the resonant component. These two integrals are expressed as in Eqs. (8) and (9).

$$\sigma_{a,b}^2 = \int J^2(n)S_{cu}(n)dn \text{ - with } 0 \leq n < n_0 \tag{8}$$

$$\sigma_{a,r}^2 = \frac{\pi n_0 S_{cu}(n_0)}{4\xi} \tag{9}$$

The spectral formulation accepts $M^* = m\int_0^H \phi(z)^2 dz$ for estimating $S_A(n)$, where m is the mass per unit length, assumed here to be constant along regular prismatic structures. The generalised mass then goes through Eqs. (2) and (6) to ensure consistency between input energy and system properties. The identified transfer function $J(n)$ will transform input (excitation) into output (response) acceleration while, by defining a cut-off frequency $n < n_0$ for integrating Eq. (7), one enables the background response components depicted in Eq. (8) to be determined. The resonant response component is then calculated with Eq. (9), which centers at the fundamental frequency of vibration, n_0, as explained by Simiu and Scanlan (1996). The design spectra result from combining results derived from Eq. (8) and (9) as $S_a = \sqrt{\sigma_{a,b}^2 + \sigma_{a,r}^2}$ once applied to a collection of oscillators whose fundamental vibrational period (T) falls within a pre-determined range, for example, $0.1s \leq T \leq 10s$. The full procedure to calculate wind design spectra is shown in Table 1.

4

Table 1 Steps to calculate wind design spectra.

Input data		Feeding into	Comment
Stage 1: Spectrum of Acceleration			
H	: Height of structure	$$\phi(z) = \left(z/H\right)^{\beta}$$	$10m \leq H \leq 500m; \beta = 1.5$
β	: Constant value		
$\phi(n)$	: Modal shape	$$M^* = m \int_0^H \phi(z)^2 dz$$	Use mass per unit volume (m_v) and plan area *(L·W)* to calculate m
m	: Mass per unit length		
A	: Area exposed to wind	$$S_A(n) = \left(\frac{q}{m}\right)^2 S_u(n)$$	Infer σ_u from $I = \sigma_u/U$, then input into $$q = \frac{1}{2}\rho C_D A(2U + \sigma_u)$$
C_D	: Drag coefficient		
I	: Turbulence intensity		
U	: Average wind velocity		
S_u	: Wind power spectrum		
Stage 2: Mechanical Admittance			
ξ	: Fraction of critical damping	$$J(n) = \frac{1}{\sqrt{(1 - r^2)^2 + 4\xi^2 r^2}}$$	Associate to the fundamental vibrational mode
r	: Frequency ratio		$r = n/n_0$
Stage 3: Cross Spectrum of Acceleration and its Generalisation			
S_A	: Spectrum of acceleration	$S_{A_{ij}}(z, n)$ $$= \frac{S_A(n)}{A^2}\psi(z)e^{-\frac{n}{1/2[U(z_i)+U(z_j)]}\sqrt{(C_y\Delta_y)^2+(C_z\Delta_z)^2}}$$	Consider $1 \leq C_w \leq 10$ For simplicity, assume linear variation of $\psi(z)$ from the reference to gradient height and calculate $U(z)$ with $$U(z) = U\left(z/z_r\right)^{\alpha}$$
C_w	: Decay constant in direction w		
α	: Power law exponent		
$U(z)$	: Velocity at height z		
$S_{A_{ij}}$	: Cross spectrum acceleration	$S_{cu}(n)$ $$= \iint_A \phi(z_i)\phi(z_j)S_{A_{ij}}(z,n)dy_i dy_j dz_i dz_j$$	Assume same amplitude of modal shape along y-axis
Stage 4: Wind Design Spectrum			
S_{cu}	: Generalised input acceleration	$$\sigma_{a,b}^2 = \int J^2(n)S_{cu}(n)dn$$ $$\sigma_{a,r}^2 = \frac{\pi n_0 S_{cu}(n_0)}{4\xi}$$	The integral running across $0 \leq n < n_0$
$J(n)$	: Transfer function		
$\sigma_{a,b}{}^2$	: Background response	$$S_a = \sqrt{\sigma_{a,b}{}^2 + \sigma_{a,r}{}^2}$$	Repeat steps for each single oscillator of period T
$\sigma_{a,r}{}^2$	: Resonant response		

3. Wind-structure interaction and its parameterisation

Eqs. (1)–(9) define structural response to wind as the multi-dimensional dynamical process represented in Eq. (10). In this equation, W represents the width of the structure, L its chord, while the ratio H / W describes the shape of the area exposed to wind.

$$\sigma_a = f(U, W, L, H/W, \xi, n_0, m, C_D, soil\ roughness, \beta) \tag{10}$$

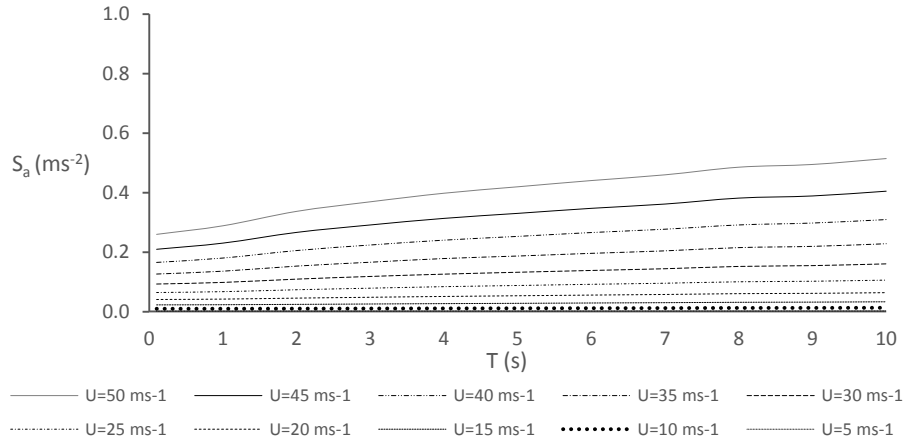The variation of wind design spectra with U, H/W, and ξ is shown in Figs. 2 and 3.

Fig. 2 Design spectra for $\xi = 0.025$, $H/W = 10$, and $W = 20$ m.

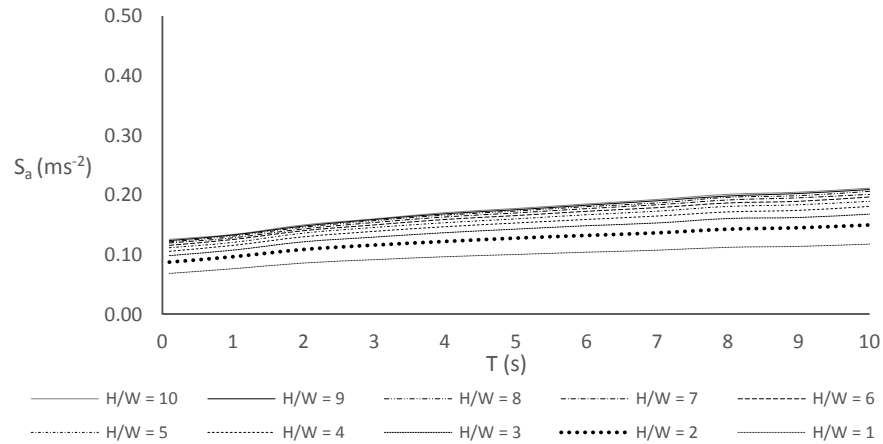Fig. 3 Design spectra for $\xi = 0.025$, $U = 25$ m s^{-1}, and $W = 10$ m.

The spectra shown in Fig. 2-3 follow the steps provided in Table 1, with the parameters dy and dz establishing the grid size for integrating Eq. (7) over the area exposed to wind. Spectral ordinates in these figures relate to a roughness length $z_0 = 0.3$ m, turbulence intensity $I = 0.295$, gradient height $H_g = 390$ m, and mass per unit volume (m_v) of 384 kg m^{-3}. These spectra show relatively large variations of pseudo-acceleration S_a with T, as a reflection of the amount of energy carried by low-frequency wind gusts. Spectral ordinates also show high sensitivity to the ratio H/W. For example, the increase of the ordinates of the response spectra for $H/W = 10$ with respect to $H/W = 1$ is well above 60% when $T = 5$ s. Moreover, spectral variations with H/W appear highly sensitive to U and W. For instance, by changing U whilst fixing $W = 10$ m, the spectral ordinates associated with $H/W = 10$ in relation to those related to $H/W = 1$ fluctuate between 40% and 80%. Conversely, by changing W whilst keeping U = 25 m s^{-1}, spectral ordinates associated to the same ratio fluctuate between 70% and 250%.

In contrast to the above, wind design spectra show smoother variations with W and ξ. Figs. 4–5 show surface-like spectra across the domains $T - W$ and $T - \xi$. In these figures, the vertical axis relates to S_a and is given in m s^{-2}.
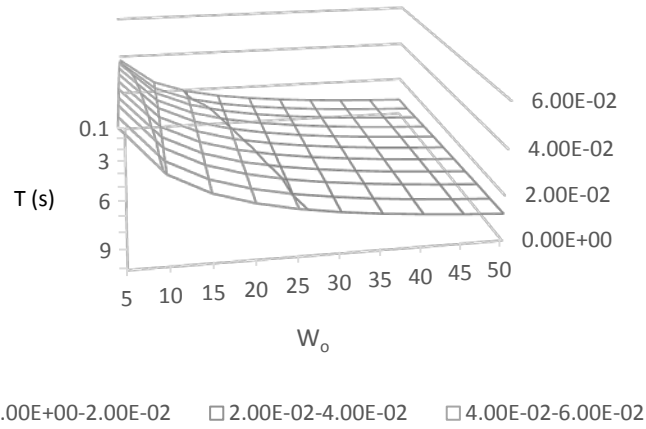
Fig. 4 Design spectra for $H/W = 10$, $U = 10$ m s^{-1}, and $\xi = 0.025$.

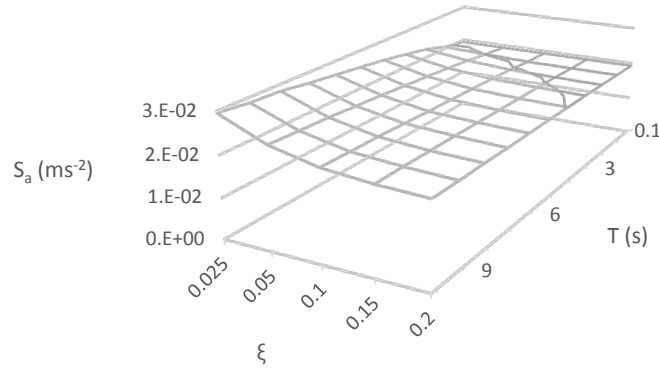Fig. 5 Design spectra for $H/W = 1$, $U = 15$ m s^{-1}, and $W = 15$ m.

From Eq. (10), some simple yet partial relationships derive between the structural response calculated for one particular site, admittance, and mass distribution.

3.1 Terrain type, admittance, and mass

The influence of soil roughness on the wind regime impacts the wind power spectrum via the gust variance. For example, the Von Karman model reads as follows:

$$\frac{n \cdot S_u(n)}{\sigma_u^2} = \frac{4nL_T/U}{(1+70.8(nL_T/U)^2)^{5/6}} \tag{11}$$

where σ_u^2 is the variance of the along-wind velocity component and L_T is the integral length scale, defined as $L_T = U \int_0^\infty \rho(\tau)d\tau$, where $\rho(\tau)$ is the autocorrelation function that changes with the time delay (τ). In this investigation, L_T was obtained from Engineering Sciences Data Unit (2000). Since terrain characteristics are captured with the turbulence intensity (I), to vary the wind design spectra with terrain type, one simply does $(IU)^2 \frac{4nL_T/U}{n \cdot (1+70.8(nL_T/U)^2)^{5/6}}$ in Eq. (11) and inputs the result into Eq. (1).

7

Furthermore, since $F = \frac{1}{2}\rho C_D A U_T^2$, if the admittance of the bluff body were to change, one simply modifies F with C_D, accordingly.

Variations of wind design spectra with mass as working out $M^* = m \int_0^H \phi(z)^2 dz$ and modal shape $\phi(z) = \left(z/H\right)^\beta$ can be quantified as follows.

$$M^* = \frac{mH}{(2\beta + 1)} \tag{12}$$

Moreover, by defining $\theta = L/W$ while letting $m = WLm_v$, where m_v is the mass per unit volume, one can determine the generalised mass as in Eq. (13).

$$M^* = \frac{W^2 \theta m_v H}{(2\beta + 1)} \tag{13}$$

The scaling factors identified above can be combined with the nonlinear estimator described in the following section to determine any new wind design spectra based on an existing one. An example of the scaling approach to determine structural response is discussed in Section 5.

4. Non-linear regression model

Figs. 4 and 5 show relatively low variations of spectral ordinates with T, W and ξ. The relationship amongst these would enable the scaling of existing wind design spectra for any combination of controlling parameters via a regression model or similar. The domains $T - W$ and $T - \xi$ can thus be simulated by a non-linear model of the form,

$$\widehat{S_a} = f(T^\lambda, W^\eta) \cdot f(T^\kappa, \xi^\iota) \tag{14}$$

Let T, W, represent regression parameters that define the surface depicted in Fig. 4. The vertical ordinate of the plane can simulate true values of design spectra through Eq. (15).

$$\widehat{S_a} = ln\theta T^\lambda + ln\gamma W^\eta + C_1 \tag{15}$$

$$e^{\widehat{S_a}} = \theta T^\lambda \cdot \gamma W^\eta \cdot C_2 \tag{16}$$

$$e^{\widehat{S_a}} = \varphi M \tag{17}$$

where $\varphi = \theta\gamma C_2$ and $M = (T + \Delta T_0)^\lambda \cdot W^\eta$, letting $T = T + \Delta T_0$ $\tag{18}$

The mean square error of this model is therefore,

$$\Sigma\left(e^{S_{a,i}} - e^{\widehat{S_{a,i}}}\right)^2 = \Sigma(e^{S_{a,i}} - \varphi\Pi_i)^2 \tag{19}$$

To minimise the error, we derive with respect to the regression parameter φ as follows:

$$\partial/\partial\varphi = 0 = \sum\Pi_i e^{S_{a,i}} - \sum\varphi\Pi_i^2 \tag{20}$$

To finally obtain,

$$\varphi = \frac{\Sigma\Pi_i e^{S_{a,i}}}{\Sigma\Pi_i^2} \tag{21}$$

The regression modelling therefore consists of fitting a plane to the domain represented in Fig. (4) through the parameters φ, λ, η and ΔT_0.

A similar approach can be derived to reproduce changes on spectral ordinates with damping. In this case, it seems convenient to model the relationship as $S_{a,\xi_r}/S_{a,\xi}$ where ξ_r is the reference damping value, set to 0.025. On that basis, the damping effect on spectral ordinates would be captured through

$$\widehat{S_{a,\xi_r}}/\widehat{S_{a,\xi}} = ln\Gamma Q \tag{22}$$

with

$$\Gamma = \frac{\Sigma Q_i e^{S_{a,i}}}{\Sigma Q_i^2} \tag{23}$$

while in this case, $Q = (T + \Delta T_1)^\kappa \cdot \xi^\iota$.

Taking as a base the design spectra represented in Fig. 5 for the specific value $\xi_r = 0.025$, Eq. (14) is now expressed as follows:

$$\widehat{S_a} = \frac{ln\varphi\Pi}{ln\Gamma Q} \tag{24}$$

valid for the interval $0.025 \leq \xi \leq 0.05$.

Fig. 6 shows examples of simulated wind design spectra calculated with Eq. (24) and the scaling factor discussed in Section 3. The base parameters are those shown in Fig. 6a, namely, $U = 20$ m s^{-1}, $W = 20$ m, $\xi = 0.025$, Terrain Type III, $L/W = 1$, and $\beta = 1.5$. Figs. 6b - 6f show changes in real and simulated spectra with mass and drag coefficient (Fig. 6b), width and drag coefficient (Figs. 6c,e), width, drag coefficient and chord to width ratio (Fig. 6d), and width (Fig. 6f).
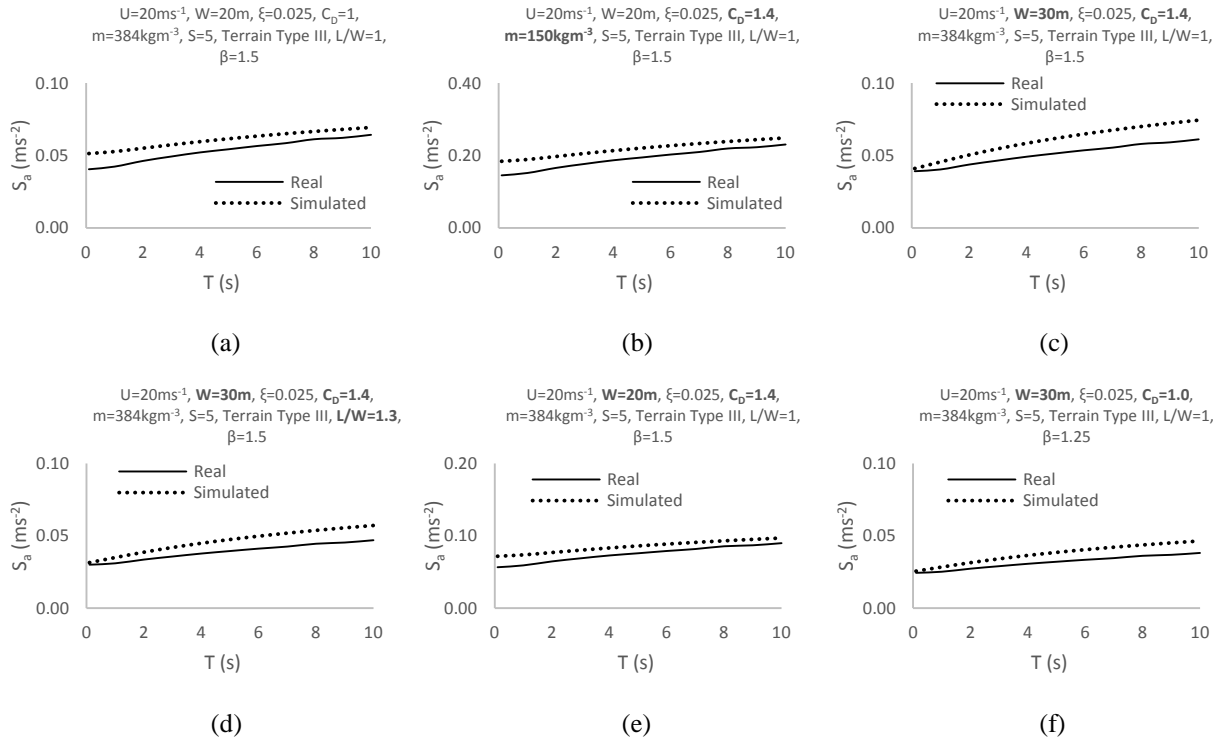

Fig. 6 Real and simulated design spectra.

The error obtained changes with the varying parameter. Tables 2-3 show values of the mean square error ($\bar{e}^2$) linked to Figs. 6a-6f with an expanded range of trials. For example, Table 2 addresses the range 10 m s^{-1} < U < 40 m s^{-1} reporting $0.004\% \leq \bar{e}^2 \leq 2.89\%$, representing between 0.33% and 12% of $\bar{e}^2/\overline{S_a}$, where $\overline{S_a}$ is the mean spectral ordinate across the domain $T - U$. That is seemingly the largest difference of the set, the smallest being the one related to the varying parameter L/W with values $\bar{e}^2$ of up to 0.044% and related $\bar{e}^2/\overline{S_a}$ of 4.3%. Table 4 shows the corresponding estimated values when the varying parameters become $Terrain\,Type, L/W$ and H/W while the scatter falls within similar ranges.

Table 2 Mean square error for varying parameters U, m and W.

U ms^{-1}	$\bar{e}^2$	$\overline{S_a}$	$\bar{e}^2/\overline{S_a}$	m_v kgm^{-3}	$\bar{e}^2$	$\overline{S_a}$	$\bar{e}^2/\overline{S_a}$	W m	$\bar{e}^2$	$\overline{S_a}$	$\bar{e}^2/\overline{S_a}$
10	0.00004	0.01203	0.00332	150	0.00840	0.19118	0.04393	10	0.00315	0.13536	0.02327
20	0.00065	0.05334	0.01226	200	0.00472	0.14338	0.03294	20	0.00128	0.07468	0.01716
30	0.00552	0.12961	0.04262	250	0.00302	0.11471	0.02636	30	0.00110	0.05062	0.02172
40	0.02890	0.24452	0.11821	300	0.00210	0.09559	0.02196	40	0.00082	0.03724	0.02202
				350	0.00155	0.08192	0.01886				
				384	0.00128	0.07468	0.01716				

Table 3 Mean square error for varying parameters $L/W, C_D$ and ξ.

L/W	$\bar{e}^2$	$\overline{S_a}$	$\bar{e}^2/\overline{S_a}$	C_D	$\bar{e}^2$	$\overline{S_a}$	$\bar{e}^2/\overline{S_a}$	ξ	$\bar{e}^2$	$\overline{S_a}$	$\bar{e}^2/\overline{S_a}$
0.5	0.00440	0.10124	0.04345	1	0.00056	0.03616	0.01552	0.01	0.00082	0.03724	0.02202
0.7	0.00224	0.07232	0.03103	1.2	0.00081	0.04339	0.01862	0.025	0.00119	0.03345	0.03560
0.9	0.00136	0.05624	0.02416	1.4	0.00110	0.05062	0.02172	0.05	0.00126	0.03137	0.04021
1.1	0.00091	0.04602	0.01975	1.6	0.00141	0.05785	0.02441	0.1	0.00118	0.03019	0.03912
1.3	0.00065	0.03894	0.01671					0.2	0.00082	0.03724	0.02202
1.5	0.00046	0.03392	0.01370								

Table 4 Mean square error for varying parameters $Terrrain\,Type, \beta$ and H/W.

$Terrain$	$\bar{e}^2$	$\overline{S_a}$	$\bar{e}^2/\overline{S_a}$	β	$\bar{e}^2$	$\overline{S_a}$	$\bar{e}^2/\overline{S_a}$	H/W	$\bar{e}^2$	$\overline{S_a}$	$\bar{e}^2/\overline{S_a}$
I	0.00009	0.01262	0.00746	1	0.00032	0.02712	0.01164	2	0.00083	0.02572	0.03224
II	0.00024	0.02020	0.01194	1.25	0.00043	0.03164	0.01358	4	0.00072	0.02699	0.02682
III	0.00082	0.03724	0.02202	1.5	0.00056	0.03616	0.01552	6	0.00210	0.02577	0.08132
IV	0.00096	0.04040	0.02388	1.75	0.00071	0.04068	0.01746	8	0.00268	0.02297	0.11652
								10	0.00145	0.01858	0.07793

5. Dynamic response of the CAARC Building

The performance of the Commonwealth Advisory Aeronautical Research Council (CAARC) benchmark building will serve to illustrate the applicability of wind design spectra. The CAARC developed this prototype in 1960 as an attempt to standardise experimental modelling. The main characteristics of the building include plan dimensions of 30.48 m x 45.72 m and a height of 183.88 m, as shown in Fig. 7. The natural frequency of the building is of 0.2 Hz along the *v* and *w* axes, the fraction of critical damping equals 0.01, and the mass per unit volume of construction is 160 kg m^{-3}.
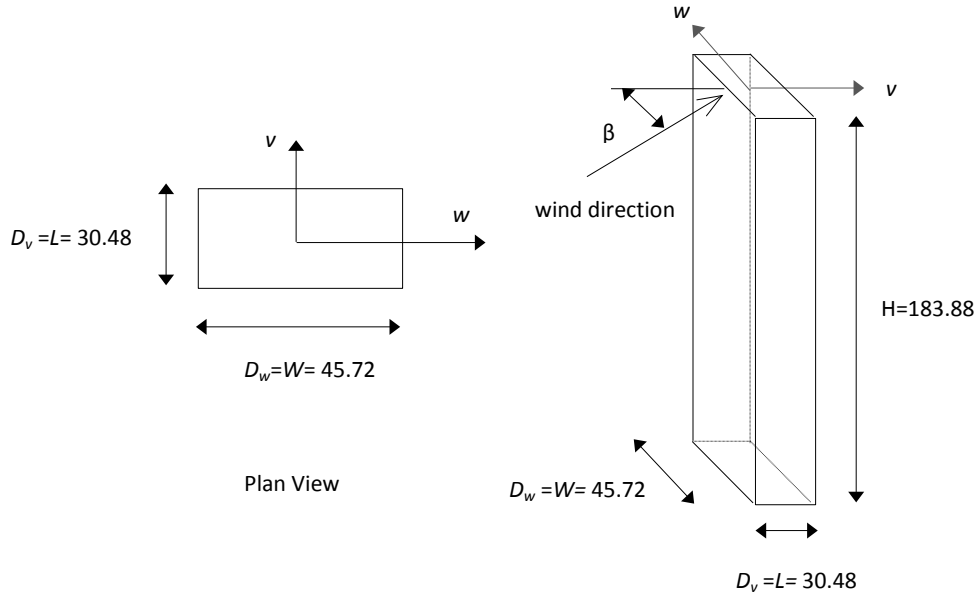
Fig. 7 The CAARC benchmark building.

In 1975, the CAARC building was experimentally tested in five different laboratories (Melbourne, 1980): the University of Western Ontario, Canada, University of Bristol, England, Monash University, Australia, and National Physical Laboratory, England (2). Details of the experimental campaign were reported by Holmes (1975), Lawson (1978), Saunders and Melbourne (1975), Walshe (1974), and Wardlaw and Moss (1970). They used a turbulence intensity at the top of the building of 0.1, which then varied linearly to measure 0.2 at $z = 10$ m (full scale equivalent), and a power-law exponent of 0.28. This parameterisation was reproduced in the present investigation. Here, the static displacement of the building was derived from the relationship $\Delta = F^*/K^*$, where F^* and K^* represent generalised force and stiffness, respectively. These are $F^* = \int_0^H f(z) \cdot \phi(z) dz$ and $K^* = 4\pi^2 n_0^2 M^*$, while the dynamic response was calculated through a modal analysis with Eq. (25), for five levels of wind average velocity covering the range 5 m s$^{-1} \leq U \leq 25$ m s^{-1}.

$$\sigma_d = \phi \frac{L*}{M*} \frac{S_a}{\omega_n^2} \tag{25a}$$

$$L^* = m \int_0^H \phi(z) dz \; ; M^* = m \int_0^H \phi(z)^2 dz \tag{25b}$$

Directly obtained (Eq. 5-8) and scaled wind design spectra (Eq. 24) were in use to assess the modelling approximation described in Sections 3 and 4. The spectral ordinates obtained are listed in Table 5.

Table 5. Spectral accelerations (m s^{-2}) calculated for the CAARC building.

wind direction	U (m s^{-1})									
	5		10		15		20		25	
	Direct	Eq. (24)	Direct	Eq. (24)	Direct	Eq. (24)	Direct	Eq. (24)	Direct	Eq. (24)
v	0.00473	0.0025	0.02172	0.0295	0.0520	0.0718	0.0997	0.1067	0.171	0.244
w	0.00211	0.0011	0.00967	0.0113	0.0232	0.0321	0.0445	0.0477	0.076	0.10

The estimated static and dynamic displacements obtained for each input acceleration are given in Table 6. The displacements corresponding to the experimental tests (Exp.) shown in Table 5 were calculated with Eq. (26) below, mapped from Melbourne (1980). In this equation, σ_k and D_k are the *rms* of displacement and dimension of the building perpendicular to the wind direction k.

$$\frac{\Delta_v}{D_v} = 3.7x10^{-4} \left(\frac{U_H}{n_0 D_w}\right)^2 ; \frac{\sigma_v}{D_v} = 3x10^{-5} \left(\frac{U_H}{n_0 D_w}\right)^3 ; \frac{\Delta_w}{D_w} = 1.2x10^{-4} \left(\frac{U_H}{n_0 D_w}\right)^2 \frac{\sigma_w}{D_w} = 9.5x10^{-6} \left(\frac{U_H}{n_0 D_w}\right)^3$$

(26)

The differences between the spectral approximations and experimental results are presented in Table 6 and Fig. 8. These results show agreement with Eq. (26). The displacements in the two directions calculated through either spectral approach are within the limits of divergence obtained experimentally. In the direction v, the divergence obtained at NAE (a) (0.0225 m) was nearly double that found through the direct spectral method (Eqs. 5-8) and exceeded by approx. 30% those generated through the spectral simulation (Eq. 23). In the direction w, the divergence of results from NAE (b) (0.0210 m) exceeded by 55% and 2.9% those found with the spectral direct and simulated methods.

Table 6. Static and dynamic responses calculated for the CAARC building.

wind direction	U_{10} (m s^{-1})	U_H (m s^{-1})	$\frac{U_H}{n_0 D_y}$	Static Response		Dynamic Response		
				$\Delta = F^*/K^*$	Exp.	Spectral Real	Spec Eq. (24)	Exp.
	5	11.28	1.234	0.0171	0.0172	0.0046	0.0024	0.0017
	10	22.56	2.469	0.0685	0.0689	0.0211	0.0287	0.0138
v	*15*	33.85	3.703	0.1541	0.1548	0.0506	0.0699	0.0465
	20	45.13	4.934	0.2740	0.2751	0.0970	0.1039	0.1101
	25	56.41	6.172	0.4281	0.4299	0.1661	0.2382	0.2151
	5	11.28	1.234	0.0084	0.0084	0.0021	0.0011	0.0008
	10	22.56	2.469	0.0336	0.0334	0.0094	0.0123	0.0065
w	*15*	33.85	3.703	0.0757	0.0752	0.0226	0.0312	0.0221
	20	45.13	4.934	0.1346	0.1337	0.0433	0.0464	0.0523
	25	56.41	6.172	0.2103	0.2089	0.0742	0.1064	0.1021

Table 6 Mean divergence (m) of all methods with respect to Eq. (26)

wind direction	Analysis	$\Delta = F^*/K^*$	Western	NAE (a)	NAE (b)	Monash	Spectral Real	Spec Eq. (24)
v	static	0.0008	0.0194	0.0391	0.0216	0.0126		
	dynamic		0.0205	0.0225	0.0075	0.0138	0.0153	0.0137
w	static	0.0006	0.0069	0.0194	0.0321	0.0153		
	dynamic		0.0157	0.0142	0.0210	0.0096	0.0081	0.0049
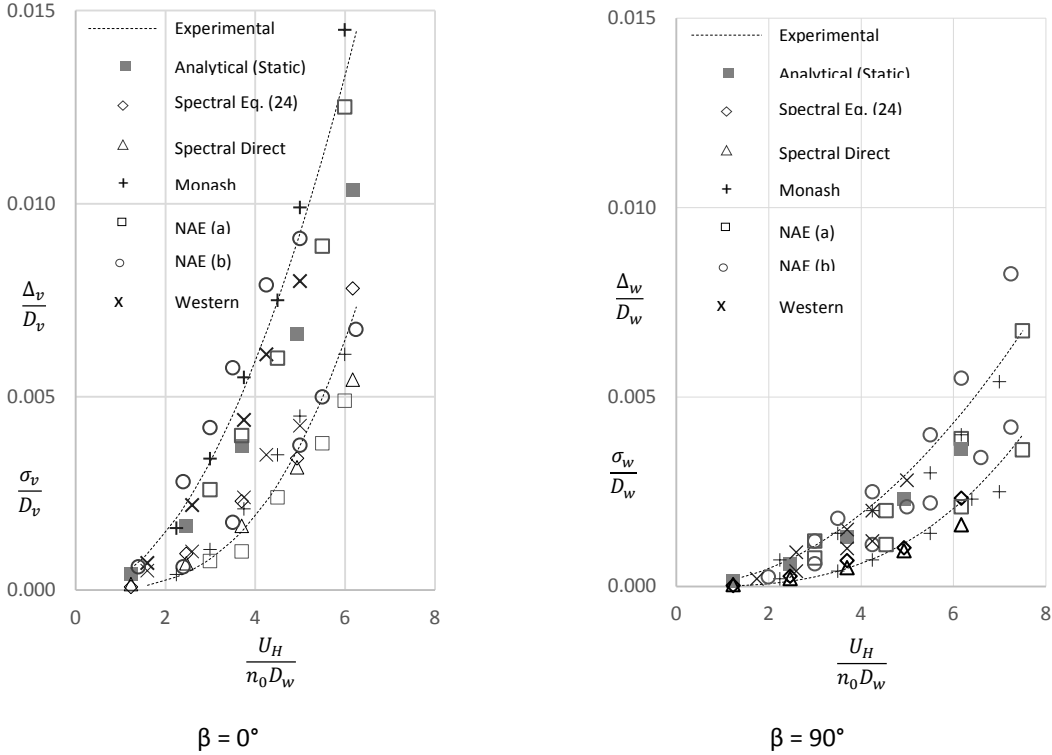
Fig. 8 Comparison of analytical results and experimental data discussed in Melbourne (1980).

In the context of the Gust Loading Factor originally developed by Davenport (1967), the peak dynamic response (R_{max}) is expressed in terms of the mean (Δ) and peak dynamic component ($g_r\sigma_r$), as in Eq. (27) — see Davenport (1967), Zhou and Kareem (1992), Chen and Kareem (2004) and Chen and Zhou (2007). The value of g_r typically ranging between 2 and 4.

$$R_{max} = \Delta + g_r\sigma_r \tag{27}$$

In this investigation, no gust response factor applied as to establish comparison with the experimental results reported by Melbourne (1980).

6. Conclusions

This paper shows that wind design spectra enable the estimation of structural dynamic response via modal analysis. This type of technology is not common practice in wind engineering as of yet, although the assessment of the method through comparison with experimental work suggests that it is viable. Identified constraints associated with the estimation of design spectra derive from the fact that a building's dynamic response strongly relates to its aerodynamic properties and location. To overcome this limitation, a non-linear simulation model that enables the scaling of existing spectra, is proposed. The scaling algorithm adjusts the terrain conditions and aerodynamic and mechanical properties of any other building. The evidence obtained through analysing a benchmark building that was experimentally tested in various laboratories around the world, indicates compatibility in the results. Previous research demonstrates that wind design spectral ordinates do not change as much across natural vibrational periods due to background wind acceleration components as they do when resonant effects are quantified. Equally, it has been observed that damping mechanisms have a higher impact on resonant response than background wind effects. The spectral approach naturally combines both turbulent wind components.

References

Chen X., Kareem A. (2004). "Equivalent static wind loads on buildings: New Model". *ASCE - J Struct Eng* **130**(10): 1425-1435.

Chen X., Zhou N. (2007). "Equivalent static wind loads on low-rise buildings based on full-scale pressure measurements". *Eng Struct* **29**: 2563–2575.

Chopra A. (1995). Dynamics of Structures: Theory and Applications to Earthquake Engineering, *Prentice Hall.*

Davenport A.G. (1967). "Gust loading factors". *American Society of Civil Engineering* **Paper 5255**: 11-34.

Davenport A.G. (1977). "The prediction of the response of structures to gusty wind". *Safety of Structures under Dynamic Loading.* Holland, Kaville, Moe and Sigbjörnsson (eds.) Tapir, Trondheim, pp. 257-284.

Dyrbye C., Hansen S. (1997). Wind Loads on Structures. *John Wiley and Sons.*

Engineering Sciences Data Unit (2000). Wind Engineering Series, Vol. 1a: 85020. *ESDU International.*

Esteva L., Rosenblueth E. (1964). "Espectros de temblores a distancias moderadas y grandes". *Boletin Sociedad Mexicana de Ingenieria Sismica* **2**:1-18.

Gong K., Chen X. (2015). "Improved modelling of equivalent static loads on wind turbine towers". *Wind and Structures* **20**(5): 609-622.

Gould P. L., Abu-Sitta S. (1980). Dynamic Response of Structures to Wind and Earthquake Loading. *Pentech Press.*

Holmes J.D. (1975). "Aeroelastic tests on the C.A.A.R.C. standard building model", *Boundary Layer Wind Tunnel Report* BLWT-1-75, University of Western Ontario, Canada, Aug.

Holmes J.D. (2002). "Effective static load distribution in wind engineering". *J. Wind Eng. Ind. Aerodyn.* **90**(2): 91-109.

Huang M.F., Li Q., Chan C.M., Lou W.J., Kwok K.C.S., Li G. (2015). "Performance-based design optimization of tall concrete framed structures subject to wind excitations". *J. Wind Eng. Ind. Aerodyn.* **139**: 70-81.

Kapersky M. (1992). "Extreme wind load distributions for linear and non-linear design". *Eng. Struct.* **14**(1): 27-34.

Lawson T.V. (1978). "The wind content of the built environment". *J. Wind Eng. Ind. Aerodyn.* **3**: 93-105.

Martinez-Vazquez P. (2016). "Wind-induced vibrations of structures using design spectra". *Int J Adv Struct Eng.* **8**:379–389.

Melbourne W.H. (1980). "Comparison of measurements on the CAARC standards tall building model in simulated model wind flows". *J. Wind Eng. Ind. Aerodyn.* **6**: 73-88.

Newmark N.M., Hall W.J. (1982). Earthquake Spectra and Design. *Earthquake Eng. Research Institute*.

Patruno L., Ricci M., Miranda S., Ubertini F. (2017). "Equivalent Static Wind Loads: Recent developments and analysis of a suspended roof". *Engineering Structures* **148**: 1-10.

Petrini, F., Ciampoli, M. (2012). Performance-based wind design of tall buildings. *Struct. Infrastruct. Eng*. **8**(10): 954–966.

Piccardo G., Solari G. (2000). "Three dimensional wind excited response of slender structures: closed form solution". *J Struct Eng*. **126**(8): 936-943.

Priestley M.J. N. (2000). "Performance based design. Proceedings of the 12th World Conference in Earthquake Engineering". *University of California, San Diego.*

Saunders J.W., Melbourne W.H. (1975). "Tall rectangular building response to cross-wind excitation", *Proc. 4th Int. Conf. on Wind Effects on Buildings and Structures*, 369-380, London.

Simiu E., Scanlan H. (1978). Wind Effects on Structures: An Introduction to Wind Engineering. *Wiley*.

Solari G. (1988). "Equivalent wind spectrum technique". *J Wind Eng Ind Aerodyn* **114**(6): 1303–1323.

Solari G. (1989). "Wind response spectrum". *J Wind Eng Ind Aerodyn* **115**(9): 2057–2073.

Sun W., Gu M., Zhou X. (2016). "Universal Equivalent Static Wind Loads of Fluctuating Wind Loads on Large-Span Roofs Based on POD Compensation". *Advances in Structural Eng.* **18**(9): 1443-1459.

Tamura Y, Katsumura A. (2012). "Universal equivalent static wind load for structures". *The Seventh International Colloquium on Bluff Body Aerodynamics and Applications (BNAA7)*. Shanghai China, Sept. 2–6.

Tanaka H., Lawen N. (1986). "Test on the CAARC standard tall building model with a length scale of 1:1000". *J. Wind Eng. Ind. Aerodyn.* **25**: 15-29.

Vickery B.J. (1970). "On the reliability of gust loading factors". *Proc. Technical Meeting Concerning Wind Loads on Buildings and Structures.* **Build. Sc. Ser. 30**. Ntl. Bureau of Standards, Washington DC 93-104.

Walshe D.E. (1974). "Tests on the standard tall building proposed by the Commonwealth Advisory Aeronautical Research Council", *NPL Report Mar Sc* **R120**, Sept.

Wardlaw R., Moss G. (1970). "A standard tall building model for the comparison of simulated natural winds in wind tunnels". *CAARC, CC 662m* Tech. **25**.

Zhou Y., Kareem A. (2001). "Gust Loading Factor: New Model". *J Struct Eng*. **127**(2): 168-175.